Title

Experimental and Theoretical Evaluation of the Thermodynamics of the Carbonation Reaction of ZIF-8 and Its Close-Packed Polymorph with Carbon Dioxide.

Journal

Journal of Physical Chemistry C, 127(39)

ISSN

1932-7447

Authors

Leonel, Gerson

Lennox, Cameron

Xu, Yizhi

et al.

Publication Date

2023-10-05

DOI

10.1021/acs.jpcc.3c04135

Peer reviewed

THE JOURNAL OF PHYSICAL CHEMISTRY C
A JOURNAL OF THE AMERICAN CHEMICAL SOCIETY

pubs.acs.org/JPCC
Article

Experimental and Theoretical Evaluation of the Thermodynamics of the Carbonation Reaction of ZIF-8 and Its Close-Packed Polymorph with Carbon Dioxide

Gerson J. Leonel, Cameron B. Lennox, Yizhi Xu, Mihails Arhangelskis,* Tomislav Friščić,* and Alexandra Navrotsky*

Cite This: J. Phys. Chem. C 2023, 127, 19520−19526

Read Online

ACCESS | Metrics & More | Article Recommendations | Supporting Information

ABSTRACT: We report the first experimental and theoretical evaluation of the thermodynamic driving force for the reaction of metal−organic framework (MOF) materials with carbon dioxide, leading to a metal−organic carbonate phase. Carbonation upon exposure of MOFs to CO_2 is a significant concern for the design and deployment of such materials in carbon storage technologies, and this work shows that the formation of a carbonate material from the popular SOD-topology framework material ZIF-8, as well as its dense-packed *dia*-topology polymorph, is significantly exothermic. With knowledge of the crystal structure of the starting and final phases in the carbonation reaction, we have also identified periodic density functional theory approaches that most closely reproduce the measured reaction enthalpies. This development now permits the use of advanced theoretical calculations to calculate the driving forces behind the carbonation of zeolitic imidazolate frameworks with reasonable accuracy.

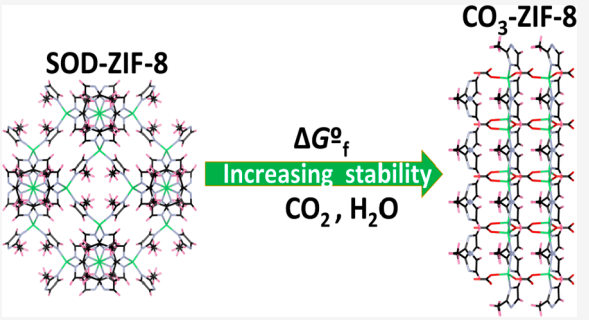

INTRODUCTION

Over the past three decades, the chemistry of metal−organic frameworks (MOFs) has become one of the central areas of advanced materials research,[1−3] with a wide range of proposed applications, from gas storage, catalysis, and light harvesting to extending shelf lives of vaccines and rocket propulsion.[4−7] The rapid development and high popularity of MOFs are to a large extent due to their inherently modular node-and-linker design,[8,9] which permits the rational development of new materials that combine previously unimaginable surface area and microporosity with specific chemical or physical properties, such as color, luminescence, conductivity, sensing ability, and more.[6,10−15] Whereas the development of new MOF designs is facilitated by concepts of reticular chemistry and, very recently, methodologies for *ab initio* crystal structure prediction (MOF-CSP),[16] the understanding and reliable design of thermodynamic stability in MOFs remains poorly explored. This is both a significant challenge and an opportunity for the further development of MOFs, as thermodynamic stability is the driving force underlying a wide range of environmental behaviors important for potential applications of MOFs, such as resistance to moisture, chemical reagents, temperature, etc.[17−21] Important insights into the relative stability of MOF polymorphs, as well as thermodynamic relationships with respect to metal precursors, can be gained from computational methods, particularly periodic density functional theory (DFT) calculations. In that context, our team has recently used a combination of solution calorimetry and periodic DFT to provide the first quantitative insights into how the thermodynamic stability of zeolitic imidazolate frameworks (ZIFs), a class of MOFs exhibiting zeolite-like topologies and based on imidazolate linkers and tetrahedral ions such as Zn^{2+}, Co^{2+}, or Cd^{2+}, is affected by changes in topology, polymorphism, and of substituents on the organic linker.[22−24] These studies have revealed that thermodynamic stability of ZIFs can be assessed through simple tabulated parameters, such as Hammett σ-constants, and even predicted from readily calculated linker parameters, such as the electrostatic surface potential (ESP) of the linker substituent.[22] Moreover, the combined use of periodic DFT and solution calorimetry measurements enabled quantitative evaluation of the accuracy of the theoretical calculations and establish that dispersion-corrected energy provides more accurate energies for ZIF structures than pure semilocal functionals. This work mainly addressed thermodynamic stability of ZIFs with respect to the parent metal oxide plus

Received: June 19, 2023
Revised: September 11, 2023
Published: September 21, 2023

https://doi.org/10.1021/acs.jpcc.3c04135
J. Phys. Chem. C 2023, 127, 19520−19526

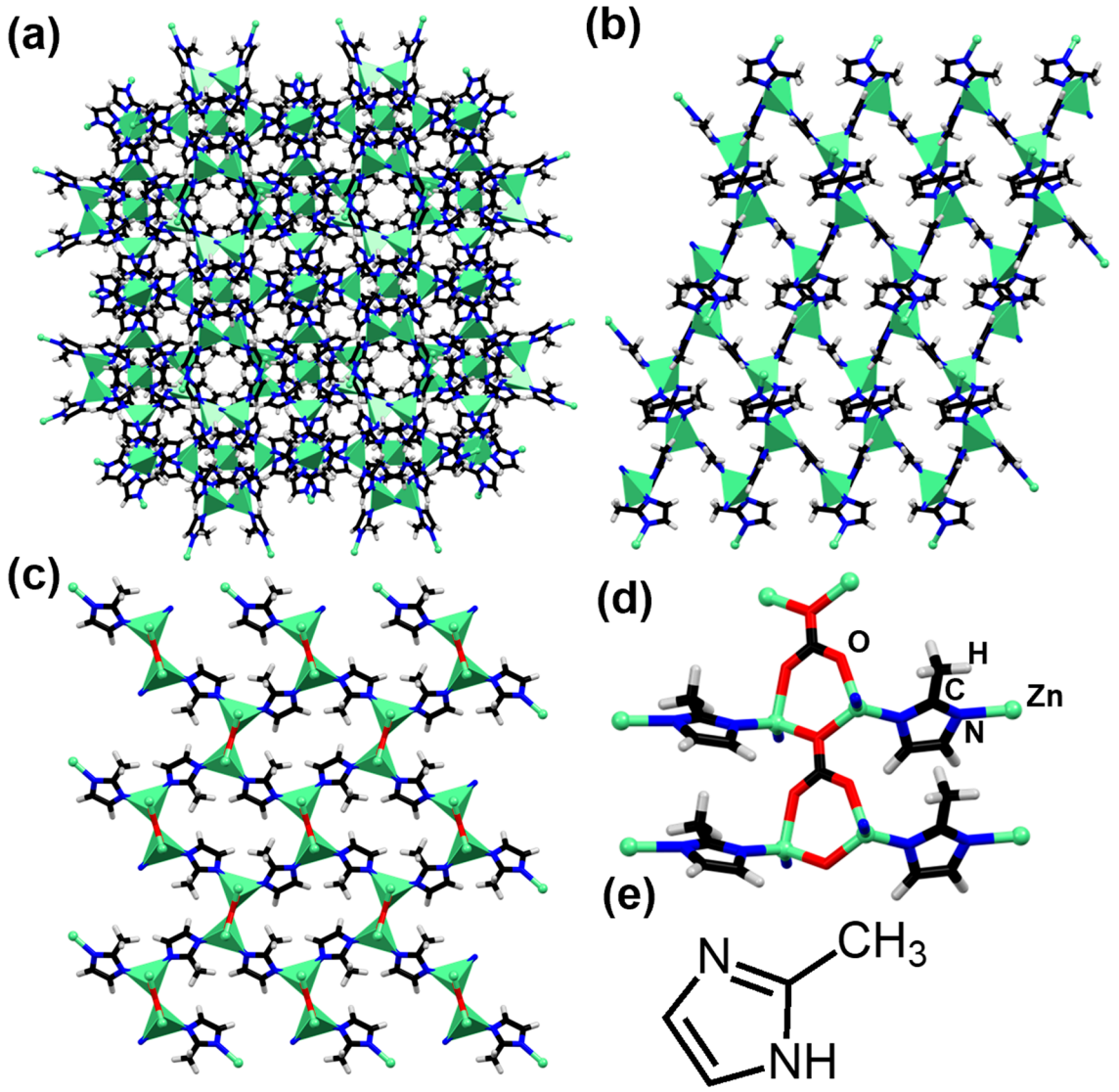

Figure 1. Structure of (a) SOD-Zn(MeIm)$_2$, (b) *dia*-Zn(MeIm)$_2$, (c) $Zn_2(MeIm)_2CO_3$, (d) carbonate and imidazolate linkers, and (e) the 2-methylimidazole (HMeIm) ligand. Zn, oxygen, carbon, hydrogen, and nitrogen atoms are depicted by green, red, black, gray, and blue spheres, respectively.

linker, providing a measure of the sensitivity of the materials toward hydrolysis. It remains important to evaluate the stability of MOFs toward a wide range of environmental factors, such as the presence of reactive gases (CO_2, SO_2, etc.).[25−28] Although one of the most prominent proposed applications of MOF materials (including ZIFs) is storage of CO_2, there have so far been no studies of their thermodynamic stability to reaction with CO_2. Reactivity with CO_2 is an important problem in MOF development, and indeed, our group has previously reported that exposure of diverse ZIFs to moist CO_2 environments leads to the formation of mixed-ligand carbonate-containing phases.[29]

We now provide the first experimental and theoretical study of the thermodynamics of the reaction of the popular, commercially relevant framework ZIF-8 (Figure 1a), based on Zn^{2+} nodes and 2-methylimidazolate ($MeIm^-$) linkers, to form the carbonate phase $Zn_2(MeIm)_2CO_3$ (Figure 1c) The reaction of ZIF-8 with moist CO_2 was previously reported to rapidly yield the $Zn_2(MeIm)_2CO_3$ phase,[29] which also forms as a side product upon mechanochemical synthesis of ZIF-8 if basic zinc carbonate is used as the metal precursor.[30]

The crystal structure of $Zn_2(MeIm)_2CO_3$ was previously determined from powder X-ray diffraction (PXRD),[30] and the data present Zn^{2+} metal centers tetrahedrally coordinated to two imidazolate and two carbonate linkers (Figure 1). Notably, the availability of crystallographic data for $Zn_2(MeIm)_2CO_3$ enabled us to develop and compare different semiempirical dispersion-corrected periodic density functional (SEDC-DFT)[31−37] approaches to evaluate the driving force for the carbonation reaction of ZIF-8 and of *dia*-Zn(MeIm)$_2$.

To the best of our knowledge, this work presents the first experimental evaluation of the thermodynamics of the reaction of an MOF with carbon dioxide. Moreover, the high degree of agreement between experimentally determined enthalpies and theoretically calculated reaction energies demonstrates, for the first time, the ability to theoretically calculate with high accuracy the driving force for MOF carbonation using periodic DFT.

https://doi.org/10.1021/acs.jpcc.3c04135
J. Phys. Chem. C 2023, 127, 19520−19526

EXPERIMENTAL METHODS

Detailed synthesis and characterization of the materials are provided as Supporting Information.

Thermodynamic Measurements. Room temperature acid solution calorimetry (in 5 N HCl) measures the heats of dissolution, from which heats of formation are calculated. Calorimetric measurements are performed in a CSC4400 isothermal microcalorimeter. The calorimeter is calibrated through the dissolution of KCl at room temperature (25 °C). The experimental procedure is well-established.[38−40]

Theoretical Calculations of Reaction Thermodynamics. Periodic DFT geometry optimization calculations are used to compute the energies of all of the individual reaction components. All geometry optimizations are performed using plane-wave periodic DFT in the code CASTEP 19.11.[41] The input files are generated using the program cif2cell from the experimentally determined crystal structures.[42] For calculating the energies of gas molecules of CO_2 and H_2O using periodic DFT, a cell of dimension 20 × 20 × 20 Å^3 is created with one molecule of H_2O and CO_2 inside to mimic the gaseous phase of these two species. Moreover, because the liquid phase water is involved in eqs 1−5, the experimentally measured enthalpy of water vaporization, which is 43.9 kJ mol^{-1} at 25 °C, is the energy used to convert from gas- to liquid-phase water. Calculations are performed with five different computational methods in order to investigate the effect of using different functionals and dispersion correction schemes on the resulting reaction energies: PBESOL functional, PBE functional with Grimme D3 dispersion correction, PBE with many-body dispersion (MBD*) correction scheme, PBE with Tkatchenko−Scheffler (TS) dispersion correction scheme, and PBESOL with TS dispersion correction scheme.[43−49] The plane-wave cutoff is set to 700 eV, and the first electronic Brillion zone is sampled with a $2\pi \times 0.07$ Å^{-1} k-point grid spacing. The ultrasoft pseudopotentials from the default CASTEP internal library are used. For the convergence of geometry optimization, the criteria of maximum energy change 2×10^{-5} eV/atom, maximum force on atom 0.05 eV/Å, maximum atom displacement 0.001 Å, and residual stress 0.01 GPa are employed. The calculated energies of all reagent and product structures for each of the periodic DFT methods are listed in Table S1. These values are used to compute the theoretical energies for the reactions describing the formation of $Zn_2(MeIm)_2CO_3$ (Table 2).The error reported for results from calorimetric experiments refers to the standard error (two standard deviations of the mean) for at least six experiments per sample. In this work, the accuracy of the experimental results is statistically significant to two decimal places, as reported in Tables 1 and 2. The DFT calculations are numerically exact, meaning that repeating the calculation provides the same numerical value; hence, the choice of significant figures for values obtained from DFT is arbitrary. In the context of this work, the number of significant figures in the results from DFT is made to be consistent with results from calorimetry.

RESULTS AND DISCUSSION

The results from calorimetric experiments (Table 1) are consistent with previous measurements for ZIF-8 and its close-packed polymorph *dia*-$Zn(MeIm)_2$ and show that formation of the $Zn_2(MeIm)_2CO_3$ is highly exothermic with respect to ZnO. Specifically, the measured enthalpy of formation (ΔH°_f)

Table 1. Enthalpies of Dissolution (ΔH_{dis}, in kJ mol^{-1}) in 5 N HCl at 25 °C and Formation from End Members (Metal Oxide and Linker)[a]

sample	ΔH_{dis} (kJ mol^{-1})	ΔH°_f (kJ mol^{-1})
HMeIm	−43.75 ± 0.59	
ZnO[50]	−72.29 ± 0.17	
H_2O[51]	−0.5	
$ZnCO_3$	0.71	
SOD-$Zn(MeIm)_2$	−138.25 ± 0.5	−21.04 ± 0.79
dia-$Zn(MeIm)_2$	−127.86 ± 1.08	−31.09 ± 1.10
$Zn_2(MeIm)_2CO_3$ (CO_3-ZIF-8)	−143.68 ± 0.43	−87.88 ± 0.74

[a]For $Zn_2(MeIm)_2CO_3$, the enthalpy of formation (ΔH°_f, in kJ mol^{-1}) is calculated relative to the metal oxide, linker, and CO_2.

for $Zn_2(MeIm)_2CO_3$ of ca. −88 kJ mol^{-1} corresponds to the enthalpy of the reaction involving ZnO, HMeIm, H_2O, and CO_2 as precursors (eq 1).

$$2ZnO(s, 298\ K) + CO_2(g, 298\ K) + 2HMeIM(s, 298\ K) \rightarrow Zn_2(MeIm)_2CO_3(s, 298\ K) + H_2O(1, 298\ K) \quad (1)$$

Compared to the ΔH°_f values for ZIF-8 and *dia*-$Zn(MeIm)_2$ (−21 and −31 kJ mol^{-1}, respectively), the new calorimetric data indicate a significantly higher enthalpic driving force for the formation of carbonate phase $Zn_2(MeIm)_2CO_3$ from ZnO plus linker than for the formation of ZIF without carbonate. The driving force for the formation of the $Zn_2(MeIm)_2CO_3$ phase becomes smaller, but still exothermic (−15 kJ mol^{-1}, Table 2), if the reaction proceeds through a modified route eq 2, with CO_2 being delivered in the form of $ZnCO_3$.

$$ZnO(s, 298\ K) + ZnCO_3(s, 298\ K) + 2HMIm(s, 298\ K) \rightarrow Zn_2(MeIm)_2CO_3(s, 298\ K) + H_2O(l, 298\ K) \quad (2)$$

This less exothermic enthalpy simply reflects the stability of ZnCO3 relative to that of ZnO + CO_2.

Besides establishing the enthalpies of formation for $Zn_2(MeIm)_2CO_3$, the obtained thermodynamic data enable evaluation of the thermodynamic driving force (eq 3) for the carbonation reaction of $Zn(MeIm)_2$ frameworks ZIF-8 and *dia*-$Zn(MeIm)_2$.

$$Zn(MeIm)_2(s, 298\ K) + \frac{1}{2}CO_2(g, 298\ K) + \frac{1}{2}H_2O(1, 298\ K) \rightarrow \frac{1}{2}Zn_2(MeIm)_2CO_3(s, 298\ K) + HMeIm(s, 298\ K) \quad (3)$$

The obtained values (Table 2) show that the conversion of ZIF-8 to $Zn_2(MeIm)_2CO_3$ is exothermic by ca. 23 kJ mol^{-1}, which is consistent with the observed rapid transformation either in moist CO_2 or upon exposure of an aqueous suspension of ZIF-8 to a flow of CO_2 gas. The reaction enthalpy is less exothermic (−13 kJ mol^{-1}) but still significant for the *dia*-$Zn(MeIm)_2$ phase. Having demonstrated a strong enthalpic driving force for the reaction of ZIF carbonation, we also explored the thermodynamics of other routes for the formation of $Zn_2(MeIm)_2CO_3$. In particular, we envisage that the formation of $Zn_2(MeIm)_2CO_3$ from SOD- and *dia*-$Zn(MeIm)_2$ frameworks could also take place by reaction with $ZnCO_3$ (eq 4) or a combination of equimolar amounts of ZnO and CO_2 as the source of carbonate (eq 5).

https://doi.org/10.1021/acs.jpcc.3c04135
J. Phys. Chem. C 2023, 127, 19520−19526

Table 2. Measured and Calculated Thermodynamic Data for the Reactions Leading to the Formation of the $Zn(MeIm)_2CO_3$ Carbonate Phase, Including Enthalpies of Formation (ΔH^o_f, in kJ mol^{-1}) and Enthalpies of Reaction Starting from ZIF-8 ($\Delta H^o_{f,ZIF\text{-}8}$, in kJ mol^{-1}) and *dia*-$Zn(MeIm)_2$ ($\Delta H^o_{f,dia}$, in kJ mol^{-1}), as Well as Corresponding Energies Based on Periodic SEDC-DFT Calculations

reaction from eq no.	reference framework	experimental (kJ mol^{-1})	PBE+D3 (kJ mol^{-1})	PBESOL (kJ mol^{-1})	PBE+MBD* (kJ mol^{-1})	PBE+TS (kJ mol^{-1})	PBESOL+TS (kJ mol^{-1})
1		−87.88 ± 0.74	−78.06	−101.37	−88.21	−83.58	−96.79
2		−14.88 ± 0.70	−26.05	−38.14	−30.80	−30.76	−15.51
3	*dia*	−12.53 ± 0.70	−39.86	−36.66	−37.30	−38.30	−53.07
3	SOD	−22.92 ± 0.44	−55.13	−29.05	−52.70	−61.96	−77.74
4	*dia*	16.53 ± 1.16	−26.88	−24.12	−23.99	−27.27	−20.19
4	SOD	6.14 ± 0.66	−42.15	−16.51	−39.40	−50.93	−44.85
5	*dia*	−56.47 ± 1.17	−78.89	−87.35	−81.41	−80.09	−101.47
5	SOD	−66.86 ± 0.68	−94.16	−79.74	−96.81	−103.75	−126.13

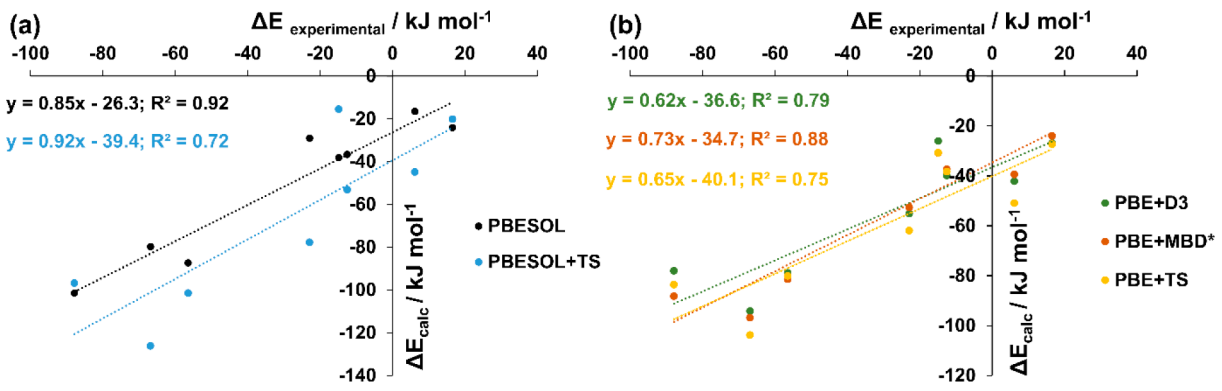

Figure 2. Linear regression plots showing the comparison between experimental and calculated reaction energies for the different periodic DFT methods: (a) PBESOL and PBESOL+TS; (b) PBE+D3, PBE+MBD*, and PBE+TS.

$$Zn(MeIm)_2(s, 298\ K) + ZnCO_3(s, 298\ K) \rightarrow Zn_2(MeIm)_2CO_3(s, 298\ K) \quad (4)$$

$$Zn(MeIm)_2(s, 298\ K) + ZnO(s, 298\ K) + CO_2(g, 298\ K)) \rightarrow Zn_2(MeIm)_2CO_3(s, 298\ K) \quad (5)$$

The thermodynamic cycles for these alternative pathways show that the reaction of $Zn(MeIm)_2$ and $ZnCO_3$ to form a carbonated ZIF phase is endothermic by ca. 6 kJ mol^{-1} (for ZIF-8) and 16 kJ mol^{-1} (for *dia*-$Zn(MeIm)_2$). This means that considering the enthalpic driving force for the reaction, the carbonate phase $Zn_2(MeIm)_2CO_3$ may be metastable toward dissociating into an equimolar mixture of $ZnCO_3$ and the corresponding ZIF. Although the entropy associated with this reaction is not known, it is likely to be small in magnitude for the reaction involving only solid phases, and the sign of the free energy change for the reaction is probably determined by the endothermic enthalpy term. In contrast, the reaction described in eq 5, where the source of additional zinc and carbonate is a combination of ZnO and CO_2, is exothermic by −67 and −57 kJ mol^{-1} for ZIF-8 and *dia*-$Zn(MeIm)_2$ as reactants, respectively. The entropy of reaction is almost certainly negative because CO_2 gas is consumed, but the sign of the free energy change is likely to be dominated by the strongly exothermic enthalpy term.[51]

With the established experimental enthalpies for the formation of $Zn_2(MeIm)_2CO_3$ via five reaction pathways, we explored the possibility to theoretically calculate the energy differences for the reactions described by eqs 1−5. Whereas we have previously demonstrated the high accuracy of periodic DFT for calculating energy differences between compositionally similar crystalline solids, the calculation of energies for reactions in eqs 1−5 is additionally challenged by the physical and chemical differences between the reaction components. For the periodic DFT calculations, we have tested the performance of DFT functionals with and without dispersion semiempirical dispersion corrections (SEDCs).[46,49,52,53] The use of SEDCs has been found essential to correctly reproduce the energy ranking of ZIF polymorphs, but it is not clear whether they will perform equally well when modeling solid state transformations involving at the same time crystalline metal−organic phases (SOD- and *dia*-$Zn(MeIm)_2$, $Zn_2(MeIm)_2CO_3$), inorganic crystalline phases (ZnO, $ZnCO_3$), and noncrystalline components CO_2(g) and H_2O(l). Modeling the thermodynamics of such reactions, therefore, requires treatment of three states of aggregation, as well as balancing the interconversions between organic and inorganic phases, where the former typically require treatment with dispersion corrections while the latter generally do not. We have previously highlighted the challenge of modeling such processes, in the context of decomposition of putative metal pentazolate frameworks and of ZIF combustion.[4,54,55] In order to achieve the best possible understanding of the performance of periodic DFT calculations for calculating reaction energies involving such diverse components, we decided to employ a wider range of methods. Besides the previously used PBE[44] functional, we also introduced its modified version PBESOL,[56] which is specifically tailored to the calculations for solid materials. Alongside these functionals, we have tested the effect of various available dispersion correction approaches, namely

https://doi.org/10.1021/acs.jpcc.3c04135
J. Phys. Chem. C 2023, 127, 19520−19526

Grimme D3,[45] Tkatchenko–Scheffler (TS),[49] and many-body dispersion (MBD*).[47−49] Because not all combinations of functionals and dispersion corrections are available in CASTEP,[41] we performed the calculations with the following methods: PBESOL, PBE+D3, PBE+MBD*, PBE+TS, and PBESOL+TS. Comparison of the calculated and experimental reaction energies revealed that the PBESOL functional without any dispersion corrections provides the best overall agreement with experiment (R^2 = 0.92, Figure 2), superior to any of the dispersion-corrected methods. However, this overall trend misses one important consideration, namely, that PBESOL incorrectly ranks the energies of the two polymorphs of $Zn(MeIm)_2$, placing the *dia* polymorph 7.61 kJ mol^{-1} above the SOD polymorph, while experimentally the *dia* structure is found to be 10.39 kJ mol^{-1} lower in energy than ZIF-8. The dispersion-corrected methods, on the other hand, have all ranked the stability of the polymorphs of $Zn(MeIm)_2$ correctly, with the best overall match between theory and experiment displayed by the PBE+MBD* method (R^2 = 0.88). The introduction of dispersion correction schemes is therefore crucial for correctly describing the relative energetic stability of MOF structures, owing to the presence of organic fragments in their structures.[57] The PBE+MBD* that was previously found to offer the best agreement with the calorimetrically measured energies of ZIF polymorphs[23] is therefore shown to also reliably characterize the energetics of the carbonation reactions of ZIFs. We attribute the superior performance of the MBD* dispersion correction to the inclusion of higher order interaction terms in this correction scheme as opposed to pairwise-only interactions considered under the Grimme D3 and TS schemes.

Typically, the formation of higher density frameworks is energetically preferred (Figure 3), suggesting that the higher density of the carbonated framework $Zn_2(MeIm)_2CO_3$ compared to parent ZIFs may contribute to its energetically favorable formation, perhaps pointing to increase in density as a plausible driving force for the reaction.[58−60] The results from this work might help explain previously observed facile carbonation of other ZIF materials[29] because the structures proceed toward thermodynamically much more stable frameworks.

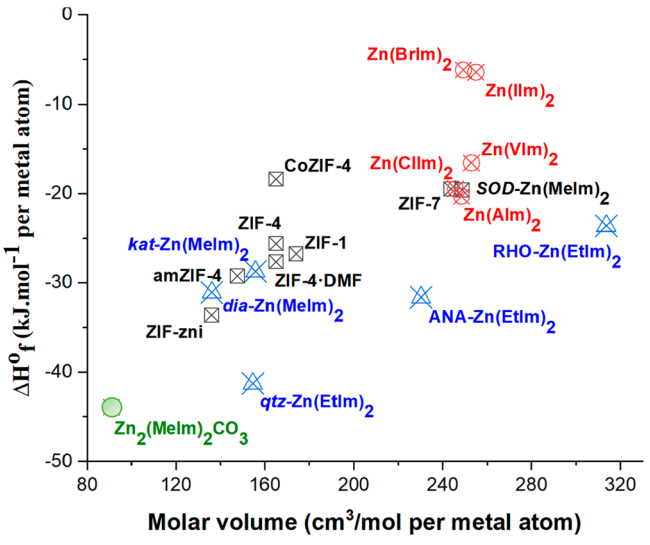

Figure 3. Change in enthalpy for the formation of ZIFs relative to their end members (metal oxide and linker). Note that $Zn_2(MeIm)_2CO_3$ employs additional CO_2 as an end member. Adapted with permission from ref 50.

CONCLUSIONS

We have provided the first experimental evaluation of the thermodynamic force underlying a MOF carbonation reaction and also investigated the dependence of this driving force on the polymorphic form of the reacting framework. With experimental enthalpies at hand, we also were able to conduct a unique study of how different theoretical approaches can evaluate the energies of the targeted MOF carbonation reaction. Our periodic DFT results match the trends for formation of $Zn_2(MeIm)_2CO_3$ via five reaction pathways in a challenging system that includes organic, metal–organic, and inorganic crystalline materials as reactants or products. Despite these challenges, the calculated reaction energies show a strong correlation with the corresponding experimental values with the best overall performance shown by the dispersion-corrected PBE+MBD* method. This work provides an opportunity to not only understand the behavior of a single system but also to begin exploring and potentially even predicting different pathways through which MOFs in general might react with CO_2.

ASSOCIATED CONTENT

Supporting Information

The Supporting Information is available free of charge at https://pubs.acs.org/doi/10.1021/acs.jpcc.3c04135.

Powder X-ray diffraction (PXRD), Fourier-transform infrared attenuated total reflectance (FTIR-ATR) spectroscopy, and thermogravimetric analysis (TGA) data as well as detailed information about the synthesis of the MOFs and other detailed experimental information (PDF)

AUTHOR INFORMATION

Corresponding Authors

Alexandra Navrotsky − *School of Molecular Sciences and Center for Materials of the Universe, Navrotsky Eyring Center for Materials of the Universe, School of Molecular Sciences, and School of Engineering of Matter, Transport, and Energy, Arizona State University, Tempe, Arizona 85287, United States;* orcid.org/0000-0002-3260-0364; Email: Alexandra.Navrotsky@ASU.edu

Tomislav Friščić − *School of Chemistry Haworth Building, University of Birmingham, Edgbaston, Birmingham B15 2TT, U.K.; Department of Chemistry, McGill University, Montreal, QC H2L 0B7, Canada;* orcid.org/0000-0002-3921-7915; Email: T.Friscic@bham.ac.uk

Mihails Arhangelskis − *Faculty of Chemistry, University of Warsaw, Warsaw 02-093, Poland;* orcid.org/0000-0003-1150-3108; Email: M.arhangelskis@uw.edu.pl

Authors

Gerson J. Leonel − *Navrotsky Eyring Center for Materials of the Universe, School of Molecular Sciences and School of Engineering of Matter, Transport, and Energy, Arizona State University, Tempe, Arizona 85287, United States*

Cameron B. Lennox − *School of Chemistry Haworth Building, University of Birmingham, Edgbaston, Birmingham*

B15 2TT, U.K.; Department of Chemistry, McGill University, Montreal, QC H2L 0B7, Canada
Yizhi Xu − *Faculty of Chemistry, University of Warsaw, Warsaw 02-093, Poland*

Complete contact information is available at: https://pubs.acs.org/10.1021/acs.jpcc.3c04135

Notes

The authors declare no competing financial interest.

■ ACKNOWLEDGMENTS

A.N. and G.L. acknowledge financial support from National Science Foundation (NSF) Partnerships for International Research and Education (PIRE) grant #1743701. Y.X. and M.A. acknowledge financial support from the National Science Center of Poland (NCN) grant 2018/31/D/ST5/03619 as well as PLGrid grant PLG/2023/016258 for the access to Ares supercomputer. T.F. and C.L. thank the support of the NSERC Discovery Grant (RGPIN-2017-06467), NSERC John C. Polanyi Award (JCP 562908-2022), Tier-1 Canada Research Chair Program (TF), NSERC CGS-D Scholarship (CBL), Leverhulme International Professorship (T.F.), and the University of Birmingham.

■ REFERENCES

(1) Ockwig, N. W.; Delgado-Friedrichs, O.; O'Keeffe, M.; Yaghi, O. M. Reticular Chemistry: Occurrence and Taxonomy of Nets and Grammar for the Design of Frameworks. *Acc. Chem. Res.* **2005**, *38* (3), 176−182.
(2) O'Keeffe, M. Design of MOFs and Intellectual Content in Reticular Chemistry: A Personal View. *Chem. Soc. Rev.* **2009**, *38* (5), 1215−1217.
(3) Chen, Z.; Hanna, S. L.; Redfern, L. R.; Alezi, D.; Islamoglu, T.; Farha, O. K. Reticular Chemistry in the Rational Synthesis of Functional Zirconium Cluster-Based MOFs. *Coord. Chem. Rev.* **2019**, *386*, 32−49.
(4) Jobin, O.; Mottillo, C.; Titi, H. M.; Marrett, J. M.; Arhangelskis, M.; Rogers, R. D.; Elzein, B.; Friščić, T.; Robert, É. Metal−Organic Frameworks as Hypergolic Additives for Hybrid Rockets. *Chem. Sci.* **2022**, *13* (12), 3424−3436.
(5) Na, K.; Choi, K. M.; Yaghi, O. M.; Somorjai, G. A. Metal Nanocrystals Embedded in Single Nanocrystals of MOFs Give Unusual Selectivity as Heterogeneous Catalysts. *Nano Lett.* **2014**, *14* (10), 5979−5983.
(6) So, M. C.; Wiederrecht, G. P.; Mondloch, J. E.; Hupp, J. T.; Farha, O. K. Metal−Organic Framework Materials for Light-Harvesting and Energy Transfer. *Chem. Commun.* **2015**, *51* (17), 3501−3510.
(7) Singh, R.; White, J. F.; de Vries, M.; Beddome, G.; Dai, M.; Bean, A. G.; Mulet, X.; Layton, D.; Doherty, C. M. Biomimetic Metal-Organic Frameworks as Protective Scaffolds for Live-Virus Encapsulation and Vaccine Stabilization. *Acta Biomater.* **2022**, *142*, 320−331.
(8) Li, M.; Li, D.; O'Keeffe, M.; Yaghi, O. M. Topological Analysis of Metal−Organic Frameworks with Polytopic Linkers and/or Multiple Building Units and the Minimal Transitivity Principle. *Chem. Rev.* **2014**, *114* (2), 1343−1370.
(9) Kalaj, M.; Cohen, S. M. Postsynthetic Modification: An Enabling Technology for the Advancement of Metal−Organic Frameworks. *ACS Cent. Sci.* **2020**, *6* (7), 1046−1057.
(10) Shen, Y.; Tissot, A.; Serre, C. Recent Progress on MOF-Based Optical Sensors for VOC Sensing. *Chem. Sci.* **2022**, *13* (47), 13978−14007.
(11) Li, C.; Zhang, L.; Chen, J.; Li, X.; Sun, J.; Zhu, J.; Wang, X.; Fu, Y. Recent Development and Applications of Electrical Conductive MOFs. *Nanoscale* **2021**, *13* (2), 485−509.
(12) Cui, Y.; Yue, Y.; Qian, G.; Chen, B. Luminescent Functional Metal−Organic Frameworks. *Chem. Rev.* **2012**, *112* (2), 1126−1162.
(13) Allendorf, M. D.; Bauer, C. A.; Bhakta, R. K.; Houk, R. J. T. Luminescent Metal−Organic Frameworks. *Chem. Soc. Rev.* **2009**, *38* (5), 1330−1352.
(14) Lee, C. Y.; Farha, O. K.; Hong, B. J.; Sarjeant, A. A.; Nguyen, S. T.; Hupp, J. T. Light-Harvesting Metal−Organic Frameworks (MOFs): Efficient Strut-to-Strut Energy Transfer in Bodipy and Porphyrin-Based MOFs. *J. Am. Chem. Soc.* **2011**, *133* (40), 15858−15861.
(15) Ettlinger, R.; Lächelt, U.; Gref, R.; Horcajada, P.; Lammers, T.; Serre, C.; Couvreur, P.; Morris, R. E.; Wuttke, S. Toxicity of Metal−Organic Framework Nanoparticles: From Essential Analyses to Potential Applications. *Chem. Soc. Rev.* **2022**, *51* (2), 464−484.
(16) Darby, J. P.; Arhangelskis, M.; Katsenis, A. D.; Marrett, J. M.; Friščić, T.; Morris, A. J. Ab Initio Prediction of Metal-Organic Framework Structures. *Chem. Mater.* **2020**, *32* (13), 5835−5844.
(17) Ding, M.; Cai, X.; Jiang, H.-L. Improving MOF Stability: Approaches and Applications. *Chem. Sci.* **2019**, *10* (44), 10209−10230.
(18) Howarth, A. J.; Liu, Y.; Li, P.; Li, Z.; Wang, T. C.; Hupp, J. T.; Farha, O. K. Chemical, Thermal and Mechanical Stabilities of Metal−Organic Frameworks. *Nat. Rev. Mater.* **2016**, *1* (3), 1−15.
(19) Rieth, A. J.; Wright, A. M.; Dincă, M. Kinetic Stability of Metal−Organic Frameworks for Corrosive and Coordinating Gas Capture. *Nat. Rev. Mater.* **2019**, *4* (11), 708−725.
(20) Nguyen, J. G.; Cohen, S. M. Moisture-Resistant and Superhydrophobic Metal−Organic Frameworks Obtained via Post-synthetic Modification. *J. Am. Chem. Soc.* **2010**, *132* (13), 4560−4561.
(21) Carter, K. P.; Ridenour, J. A.; Kalaj, M.; Cahill, C. L. A Thorium Metal-Organic Framework with Outstanding Thermal and Chemical Stability. *Chem. − Eur. J.* **2019**, *25* (29), 7114−7118.
(22) Novendra, N.; Marrett, J. M.; Katsenis, A. D.; Titi, H. M.; Arhangelskis, M.; Friščić, T.; Navrotsky, A. Linker Substituents Control the Thermodynamic Stability in Metal−Organic Frameworks. *J. Am. Chem. Soc.* **2020**, *142* (52), 21720−21729.
(23) Arhangelskis, M.; Katsenis, A. D.; Novendra, N.; Akimbekov, Z.; Gandrath, D.; Marrett, J. M.; Ayoub, G.; Morris, A. J.; Farha, O. K.; Friščić, T.; et al. Theoretical Prediction and Experimental Evaluation of Topological Landscape and Thermodynamic Stability of a Fluorinated Zeolitic Imidazolate Framework. *Chem. Mater.* **2019**, *31* (10), 3777−3783.
(24) Friščić, T.; Jones, W. Recent Advances in Understanding the Mechanism of Cocrystal Formation via Grinding. *Cryst. Growth Des.* **2009**, *9* (3), 1621−1637.
(25) Bhattacharyya, S.; Han, R.; Kim, W.-G.; Chiang, Y.; Jayachandrababu, K. C.; Hungerford, J. T.; Dutzer, M. R.; Ma, C.; Walton, K. S.; Sholl, D. S.; et al. Acid Gas Stability of Zeolitic Imidazolate Frameworks: Generalized Kinetic and Thermodynamic Characteristics. *Chem. Mater.* **2018**, *30* (12), 4089−4101.
(26) Cui, K.; Nair, S.; Sholl, D. S.; Schmidt, J. R. Kinetic Model of Acid Gas Induced Defect Propagation in Zeolitic Imidazolate Frameworks. *J. Phys. Chem. Lett.* **2022**, *13* (28), 6541−6548.
(27) Bhattacharyya, S.; Sholl, D. S.; Nair, S. Quantitative Correlations for the Durability of Zeolitic Imidazolate Frameworks in Humid SO2. *Ind. Eng. Chem. Res.* **2020**, *59* (1), 245−252.
(28) Bhattacharyya, S.; Han, R.; Joshi, J. N.; Zhu, G.; Lively, R. P.; Walton, K. S.; Sholl, D. S.; Nair, S. Stability of Zeolitic Imidazolate Frameworks in NO2. *J. Phys. Chem. C* **2019**, *123* (4), 2336−2346.
(29) Mottillo, C.; Friščić, T. Carbon Dioxide Sensitivity of Zeolitic Imidazolate Frameworks. *Angew. Chem.* **2014**, *126* (29), 7601−7604.
(30) Brekalo, I.; Yuan, W.; Mottillo, C.; Lu, Y.; Zhang, Y.; Casaban, J.; Travis Holman, K.; L. James, S.; Duarte, F.; Andrew Williams, P.; et al. Manometric Real-Time Studies of the Mechanochemical Synthesis of Zeolitic Imidazolate Frameworks. *Chem. Sci.* **2020**, *11* (8), 2141−2147.
(31) Evans, J. D.; Fraux, G.; Gaillac, R.; Kohen, D.; Trousselet, F.; Vanson, J.-M.; Coudert, F.-X. Computational Chemistry Methods for Nanoporous Materials. *Chem. Mater.* **2017**, *29* (1), 199−212.

(32) Duarte Rodrigues, A.; Fahsi, K.; Dumail, X.; Masquelez, N.; van der Lee, A.; Mallet-Ladeira, S.; Sibille, R.; Filhol, J.-S.; Dutremez, S. G. Joint Experimental and Computational Investigation of the Flexibility of a Diacetylene-Based Mixed-Linker MOF: Revealing the Existence of Two Low-Temperature Phase Transitions and the Presence of Colossal Positive and Giant Negative Thermal Expansions. *Chem. – Eur. J.* **2018**, *24* (7), 1586–1605.
(33) Baburin, I. A.; Leoni, S. The Energy Landscapes of Zeolitic Imidazolate Frameworks (ZIFs): Towards Quantifying the Presence of Substituents on the Imidazole Ring. *J. Mater. Chem.* **2012**, *22* (20), 10152–10154.
(34) Witman, M.; Ling, S.; Gladysiak, A.; Stylianou, K. C.; Smit, B.; Slater, B.; Haranczyk, M. Rational Design of a Low-Cost, High-Performance Metal–Organic Framework for Hydrogen Storage and Carbon Capture. *J. Phys. Chem. C* **2017**, *121* (2), 1171–1181.
(35) Nazarian, D.; Camp, J. S.; Chung, Y. G.; Snurr, R. Q.; Sholl, D. S. Large-Scale Refinement of Metal–Organic Framework Structures Using Density Functional Theory. *Chem. Mater.* **2017**, *29* (6), 2521–2528.
(36) Tan, J.-C.; Civalleri, B.; Erba, A.; Albanese, E. Quantum Mechanical Predictions to Elucidate the Anisotropic Elastic Properties of Zeolitic Imidazolate Frameworks: ZIF-4 vs. ZIF-Zni. *CrystEngComm* **2015**, *17* (2), 375–382.
(37) Lewis, D. W.; Ruiz-Salvador, A. R.; Gómez, A.; Rodriguez-Albelo, L. M.; Coudert, F.-X.; Slater, B.; Cheetham, A. K.; Mellot-Draznieks, C. Zeolitic Imidazole Frameworks: Structural and Energetics Trends Compared with Their Zeolite Analogues. *CrystEngComm* **2009**, *11* (11), 2272–2276.
(38) Huskic, I.; Novendra, N.; Lim, D.-W.; Topic, F.; Titi, H. M.; Pekov, I. V.; Krivovichev, S. V.; Navrotsky, A.; Kitagawa, H.; Friscic, T. Functionality in Metal–Organic Framework Minerals: Proton Conductivity, Stability and Potential for Polymorphism. *Chem. Sci.* **2019**, *10* (18), 4923–4929.
(39) Huskić, I.; Novendra, N.; Lim, D.-W.; Topic, F.; Titi, H. M.; Pekov, I.; Krivovichev, S.; Navrotsky, A.; Kitagawa, H.; Friscic, T. Proton Conductivity, Stability and Potential for Polymorphism in Metal-Organic Framework Minerals, 2018.
(40) Bhunia, M. K.; Hughes, J. T.; Fettinger, J. C.; Navrotsky, A. Thermochemistry of Paddle Wheel MOFs: Cu-HKUST-1 and Zn-HKUST-1. *Langmuir* **2013**, *29* (25), 8140–8145.
(41) Clark, S. J.; Segall, M. D.; Pickard, C. J.; Hasnip, P. J.; Probert, M. I. J.; Refson, K.; Payne, M. C. First Principles Methods Using CASTEP. *Z. Für Krist. - Cryst. Mater.* **2005**, *220* (5–6), 567–570.
(42) Björkman, T. CIF2Cell: Generating Geometries for Electronic Structure Programs. *Comput. Phys. Commun.* **2011**, *182* (5), 1183–1186.
(43) Spink, C.; Wadsö, I. In *Methods of Biochemical Analysis*; Glick, D., Ed.; Wiley: Oxford, 1976; Vol. *23*, p 123.
(44) Perdew, J. P.; Burke, K.; Ernzerhof, M. Generalized Gradient Approximation Made Simple. *Phys. Rev. Lett.* **1996**, *77* (18), 3865–3868.
(45) Grimme, S.; Antony, J.; Ehrlich, S.; Krieg, H. A Consistent and Accurate Ab Initio Parametrization of Density Functional Dispersion Correction (DFT-D) for the 94 Elements H-Pu. *J. Chem. Phys.* **2010**, *132* (15), No. 154104.
(46) Tkatchenko, A.; DiStasio, R. A.; Car, R.; Scheffler, M. Accurate and Efficient Method for Many-Body van Der Waals Interactions. *Phys. Rev. Lett.* **2012**, *108* (23), No. 236402.
(47) Ambrosetti, A.; Reilly, A. M.; DiStasio, R. A., Jr.; Tkatchenko, A. Long-Range Correlation Energy Calculated from Coupled Atomic Response Functions. *J. Chem. Phys.* **2014**, *140* (18), No. 18A508.
(48) Reilly, A. M.; Tkatchenko, A. Van Der Waals Dispersion Interactions in Molecular Materials: Beyond Pairwise Additivity. *Chem. Sci.* **2015**, *6* (6), 3289–3301.
(49) Tkatchenko, A.; Scheffler, M. Accurate Molecular Van Der Waals Interactions from Ground-State Electron Density and Free-Atom Reference Data. *Phys. Rev. Lett.* **2009**, *102* (7), No. 073005.
(50) Hughes, J. T.; Bennett, T. D.; Cheetham, A. K.; Navrotsky, A. Thermochemistry of Zeolitic Imidazolate Frameworks of Varying Porosity. *J. Am. Chem. Soc.* **2013**, *135* (2), 598–601.
(51) Akimbekov, Z.; Katsenis, A. D.; Nagabhushana, G. P.; Ayoub, G.; Arhangelskis, M.; Morris, A. J.; Friščić, T.; Navrotsky, A. Experimental and Theoretical Evaluation of the Stability of True MOF Polymorphs Explains Their Mechanochemical Interconversions. *J. Am. Chem. Soc.* **2017**, *139* (23), 7952–7957.
(52) Grimme, S. Semiempirical GGA-type density functional constructed with a long-range dispersion correction. *J. Comput. Chem.* **2006**, *27* (15), 1787–1799.
(53) Ehrlich, S.; Moellmann, J.; Reckien, W.; Bredow, T.; Grimme, S. System-Dependent Dispersion Coefficients for the DFT-D3 Treatment of Adsorption Processes on Ionic Surfaces. *ChemPhysChem* **2011**, *12* (17), 3414–3420.
(54) Arhangelskis, M.; Katsenis, A. D.; Morris, A. J.; Friščić, T. Computational Evaluation of Metal Pentazolate Frameworks: Inorganic Analogues of Azolate Metal–Organic Frameworks. *Chem. Sci.* **2018**, *9* (13), 3367–3375.
(55) Titi, H. M.; Marrett, J. M.; Dayaker, G.; Arhangelskis, M.; Mottillo, C.; Morris, A. J.; Rachiero, G. P.; Friščić, T.; Rogers, R. D. Hypergolic Zeolitic Imidazolate Frameworks (ZIFs) as next-Generation Solid Fuels: Unlocking the Latent Energetic Behavior of ZIFs. *Sci. Adv.* **2019**, *5* (4), No. eaav9044.
(56) Perdew, J. P.; Ruzsinszky, A.; Csonka, G. I.; Vydrov, O. A.; Scuseria, G. E.; Constantin, L. A.; Zhou, X.; Burke, K. Restoring the Density-Gradient Expansion for Exchange in Solids and Surfaces. *Phys. Rev. Lett.* **2008**, *100* (13), No. 136406.
(57) Galvelis, R.; Slater, B.; Chaudret, R.; Creton, B.; Nieto-Draghi, C.; Mellot-Draznieks, C. Impact of Functionalized Linkers on the Energy Landscape of ZIFs. *CrystEngComm* **2013**, *15* (45), 9603–9612.
(58) Tan, J. C.; Bennett, T. D.; Cheetham, A. K. Chemical Structure, Network Topology, and Porosity Effects on the Mechanical Properties of Zeolitic Imidazolate Frameworks. *Proc. Natl. Acad. Sci. U. S. A.* **2010**, *107* (22), 9938–9943.
(59) Katsenis, A. D.; Puškarić, A.; Štrukil, V.; Mottillo, C.; Julien, P. A.; Užarević, K.; Pham, M.-H.; Do, T.-O.; Kimber, S. A. J.; Lazić, P.; et al. In Situ X-Ray Diffraction Monitoring of a Mechanochemical Reaction Reveals a Unique Topology Metal-Organic Framework. *Nat. Commun.* **2015**, *6* (1), 6662.
(60) Basnayake, S. A.; Su, J.; Zou, X.; Balkus, K. J. Carbonate-Based Zeolitic Imidazolate Framework for Highly Selective CO_2 Capture. *Inorg. Chem.* **2015**, *54* (4), 1816–1821.

NOTE ADDED AFTER ASAP PUBLICATION

This paper was published ASAP on September 21, 2023, with the incorrect spelling of Cameron B. Lennox's name. The corrected version was reposted on October 5, 2023.

https://doi.org/10.1021/acs.jpcc.3c04135
J. Phys. Chem. C 2023, 127, 19520–19526